Smart Materials and Structures

PAPER

Vibration-based inverse graphical technique for thickness estimation of bulk acoustic wave (BAW) resonators: application for corrosion monitoring of sacrificial anodes

To cite this article: Jeslin Thalapil *et al* 2021 *Smart Mater. Struct.* **30** 055015

IOP Publishing Smart Materials and Structures
Smart Mater. Struct. **30** (2021) 055015 (11pp) https://doi.org/10.1088/1361-665X/abefb4

Vibration-based inverse graphical technique for thickness estimation of bulk acoustic wave (BAW) resonators: application for corrosion monitoring of sacrificial anodes

Jeslin Thalapil[1], Durgesh Tamhane[1], Sauvik Banerjee[2,*] and Siddharth Tallur[1,*]

[1] Department of Electrical Engineering, Indian Institute of Technology Bombay, Mumbai 400076, MH, India
[2] Department of Civil Engineering, Indian Institute of Technology Bombay, Mumbai 400076, MH, India

E-mail: sauvik@civil.iitb.ac.in and stallur@ee.iitb.ac.in

Received 23 December 2020, revised 13 February 2021
Accepted for publication 17 March 2021
Published 16 April 2021

Abstract

Resonant acoustic sensors have been used in a variety of applications that leverage the large sensitivity of mechanical resonance frequency to shift in geometric or mechanical properties of the sensor induced by the measurand. In applications such as structural health monitoring, accurate damage quantification requires development of precise models for resonator-measurand interactions or advanced system identification or optimization algorithms. In this paper, we utilize a graphical technique originally proposed for damage assessment in beams, to determine the extent of corrosion of sacrificial zinc anode discs instrumented with piezoelectric transducers. We develop analytical models for expressing natural resonance frequencies of the radial and transverse vibration modes of a disc in terms of material and geometric properties of its constituent elements. The underlying parameters (in this case, the thicknesses of the zinc and zinc oxide films) are extracted from measured resonance frequencies by finding roots of the characteristic determinant of these modes through graphical technique. Even though accelerated corrosion induced by impressed current results in non-uniform corrosion of the anode, the graphical technique with uniform-corrosion model shows excellent agreement with experimental results and is suitable for in-situ monitoring of sacrificial anodes used in cathodic protection systems. This technique requires no calibration or model of corrosion dynamics, and is computationally inexpensive unlike optimization techniques.

Supplementary material for this article is available online

Keywords: structural health monitoring, corrosion monitoring, frequency based graphical inverse technique, cathodic protection system

(Some figures may appear in colour only in the online journal)

* Authors to whom any correspondence should be addressed.

1. Introduction

Bulk acoustic resonators have been used for monitoring thickness of thin films, primarily for applications in gravimetric biosensing and chemical sensing [1–5]. These sensors leverage the impact of thickness change of the structure (due to agglomeration or removal of material) on the resonance frequency of a bulk acoustic resonant mode of the structure. While capacitive and piezoelectric transduction techniques are suitable for micromachined Micro-Electro-Mechanical Systems (MEMS) resonators, the shift in resonance frequency can also be observed by attaching a piezoelectric (e.g. lead zirconate titanate—PZT) transducer to the structure and monitoring the electro-mechanical impedance (EMI) spectrum of the transducer. With the advent of the internet of things, this technique has found several applications in non-destructive evaluation and structural health monitoring (SHM) of civil infrastructure [6–8]. The versatility of PZT based EMI measurements has been supported with various modeling efforts to deterministically ascertain the change in geometric dimensions of the structure from resonance frequency measurements [9–11]. Analytical formulations based on the Kirchhoff plate theory are valid for structures that can be approximated as thin plates, but show large deviation as compared to finite element analysis (FEA) and experimental results in practical applications [10]. Moreover, models for structures with multi-layered thin films of different materials typically assume identical lateral dimensions and acoustic impedance for the various materials [11, 12], which may not always be the case.

Vibration based SHM techniques rely on the change of local stiffness which results in changes in dynamic parameters such as natural frequencies, mode shapes and damping ratios to detect and assess damage. The monitoring of mode shapes requires measurements at multiple locations, is time consuming and prone to noise. Damping parameters are sensitive to environmental conditions such as humidity and temperature, and are difficult to measure. In comparison, natural frequencies require only single-point measurement and can be monitored with greater accuracy, ease and reliability [13]. In context of SHM, the 'forward problem' involves determination of natural frequencies of vibration of a structure with knowledge of geometry, boundary conditions and damage or corrosion details. In the case of the 'inverse problem', damage quantification is obtained through knowledge of geometry, boundary conditions and changes in natural frequency [14]. Frequency based damage detection have been successfully used for determination of delamination in composite beams, and location and size of cracks in beams. The quantification of delamination or crack from measurements of shift in resonance frequency requires us to find the solution of the inverse problem by solving a set of non-linear simultaneous equations. Several analytical, FEA and optimization based techniques have been reported in literature to address the inverse problem [15–18]. Solving for several unknown parameters requires knowledge of the underlying physical mechanisms governing the parameters, or advanced system identification or optimization techniques such as neural networks or genetic algorithms [19–22]. If damage quantification (e.g. location and depth of transverse crack in a beam) can be represented with only one or two parameters, then graphical technique can be employed to effectively estimate the parameters from resonance frequency measurements. The graphical technique was first introduced to predict the size and location of cracks by plotting crack size index versus crack location for the first three resonance modes of a straight bar [23]. While the graphical technique is computationally inexpensive and can directly solve the inverse problem without iterations or network training (unlike optimization techniques or neural networks) [24], its application is restricted to problems that require solving for no more than three variables. Applications of the graphical technique in SHM reported in literature include prediction of delamination in beams [24], determination of transverse cracks [25] and longitudinal cracks in isotropic beams [26], as well as detection of longitudinal, L-type and inverted T-cracks in isotropic and bi-material beams [14].

As in case of cracks or delamination in beams, onset of corrosion affects stiffness of a structure, in turn resulting in shift in the corresponding natural resonance frequencies. Recently, we reported EMI measurement-based technique to quantify extent of corrosion of a zinc sacrificial anode without manual intervention, supported with an analytical model for discerning the extent of corrosion by monitoring shift in resonance frequency for in-plane radial expansion mode of the disc [27]. Sacrificial anodes are employed in cathodic protection system due to their preferential corrosion affinity relative to the metal to be protected. The resonance frequency variation with increasing degree of corrosion exhibits large nonlinearity due to partial delamination of the corrosion product (zinc oxide) from the disc. Estimation of the extent of corrosion of the zinc disc thus requires knowledge of the mechanism (i.e. mathematical representation of the corrosion and delamination dynamics) to accurately capture the nonlinearity. In this work we develop an alternate technique to estimate the extent of corrosion of sacrificial anodes employed as resonant sensors by utilizing the graphical technique applied to two modes of vibration of the disc; namely the radial expansion mode and the fundamental out-of-plane (transverse or 'trampoline') vibration mode of the disc. The technique is validated through extensive FEA simulations, that indicate consistently $<5\%$ error in the estimated thickness of the corroded (zinc oxide) and uncorroded (zinc) layers. The graphical technique also shows excellent performance when applied to resonance frequency values obtained from experimental measurements conducted with an impressed-current based accelerated corrosion system. By utilizing resonance frequency measurements of two vibration modes, this technique can be readily applied to directly estimate the extent of corrosion, without the need to develop mathematical models for corrosion and delamination dynamics or in-field calibration. The remainder of this paper is organized as follows: section 2 provides detailed derivation of analytical models for expressing natural resonance frequencies of the radial and transverse vibration modes of a circular plate in terms of material and geometric properties of its constituent elements, section 3 describes the graphical technique used to determine thicknesses of the corroded and uncorroded layers from the resonance frequencies, section 4 provides results on

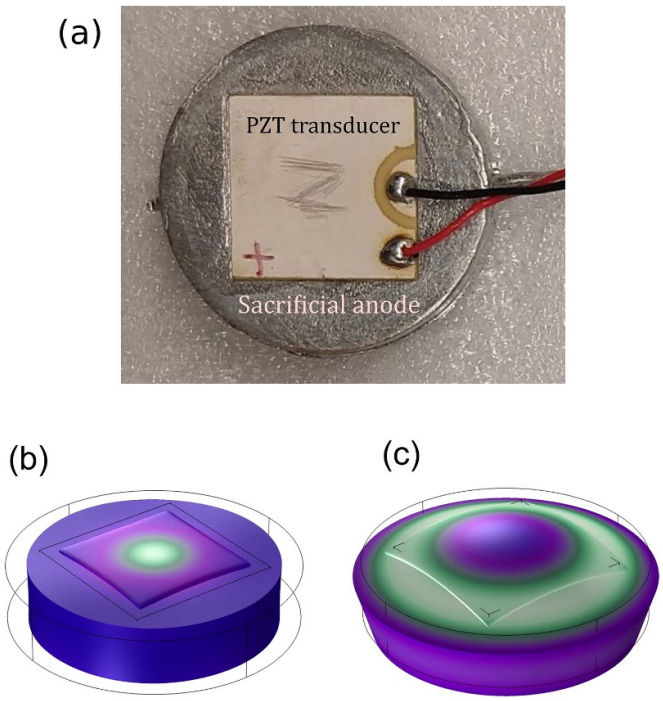

Figure 1. (a) Photograph of PZT transducer bonded to zinc sacrificial anode. The extent of corrosion of the anode is estimated by tracking the resonance frequencies of two bulk resonance modes of the structure, namely: (b) fundamental radial mode and (c) fundamental transverse mode of vibration.

validation of the graphical technique against FEA and experimental measurements, and section 5 provides a discussion of results and conclusion.

2. Mathematical formulation

We present below an analytical model for obtaining the resonance frequency of two bulk acoustic resonance modes of a circular plate. The model also incorporates a square shaped PZT transducer affixed to the plate. The structure chosen for this analysis is based on the materials used for performing experiments to validate the model, namely: cylindrical zinc sacrificial anode (Canode, Krishna Conchem Products Pvt. Ltd) of diameter 3.6 cm and thickness 0.73 cm, and PZT-5 H transducer of dimensions $20 \times 20 \times 0.4$ mm^3 (SP-5 H, Sparkler Ceramics Pvt. Ltd). Figure 1 shows a photograph of the sensor assembly, and mode shapes of the two acoustic modes utilized in this study.

2.1. Mathematical formulation for axial in-plane vibration of circular plates

We have employed a square-shaped PZT transducer in our experiments, as shown in figure 1. While a circular shaped PZT transducer is preferred, we utilized square shaped PZT transducer due to lack of availability of circular PZT at the time of performing the experiments. However, in order to simplify the mathematical formulation, we model the square PZT transducer as an equivalent circular-shaped PZT transducer so that

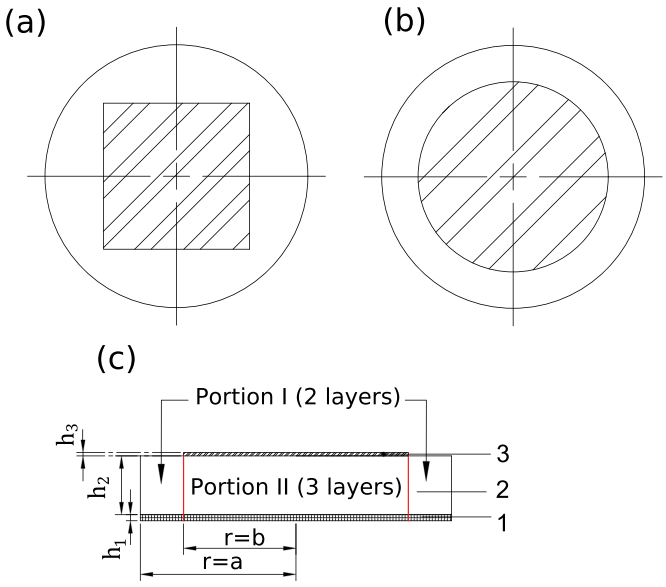

Figure 2. (a) 2D (top) view of square shaped PZT transducer on circular sacrificial anode, (b) 2D view of equivalent circular PZT transducer (of radius given in equation (1)) on sacrificial anode, and (c) cross-sectional view of the circular anode with equivalent circular PZT transducer on top surface and uniformly formed oxide layer on bottom surface. The suffixes 1, 2 and 3 denote oxide (ZnO) layer, metal (Zn) layer and PZT transducer respectively.

interface boundary condition in cylindrical coordinates can be established. The radius of the equivalent circular PZT transducer is given as [27]:

$$a_T = L\frac{\beta_T}{\pi}. \tag{1}$$

The PZT transducer used in our experiment is square-shaped with edge length 20 mm, that therefore corresponds to an equivalent circular PZT transducer with radius 13 mm [27]. The resonance frequencies of the fundamental radial and transverse modes of these two equivalent structures shown in figures 2(a) and (b) computed using FEA in COMSOL Multiphysics show excellent mutual agreement: 69.42 and 69.44 kHz for fundamental radial mode, and 30.49 and 30.52 kHz for fundamental transverse mode, for the structure with square PZT and equivalent circular PZT transducer respectively.

Vibration analysis of the corroded zinc plate with the PZT transducer is carried out by modeling the structure as a composite of two portions as shown in figure 2(c). The analytical model is formulated using 'constrained model theory' [28] where the layers are considered to be perfectly 'bonded' with each other i.e. the layers have equal radial and transverse displacements and that there is no inter-layer slip. This assumption is consistent with the experimental observation during the initial phases of corrosion [29] and there is no delamination between the layers. Thus, the structure can be divided into two portions namely: Portion I: Two layered region − Zn + ZnO, and Portion II: Three layered region − Zn + ZnO + equivalent circular PZT transducer. For a simplified vibration analysis of

this structure, the following assumptions are made: all materials are assumed to be isotropic, and corrosion is assumed to occur uniformly across the bottom surface of the zinc anode.

For the two layer (zinc and zinc oxide) circular plate with equivalent circular PZT patch undergoing axisymmetric in-plane radial vibration, the free edge boundary condition at $r = a$ is $N_{r1} = 0$ (zero radial force) i.e. $\frac{\partial U_1}{\partial r}\Big|_{r=a} + \nu_{1eq}\frac{U_1}{r}\Big|_{r=a} = 0$. At the interface between Portion I and Portion II at $r = b$, there exists continuity of radial displacement and radial forces, i.e. $U_1(r=b) = U_2(r=b)$ and $N_{r1}\Big|_{r=b} = N_{r2}\Big|_{r=b}$. Substituting the expressions for displacements in the above equations, a 3×3 characteristic determinant is obtained as below:

$$\Delta_R = \begin{vmatrix} K_{11} & K_{12} & K_{13} \\ K_{21} & K_{22} & K_{23} \\ K_{31} & K_{32} & K_{33} \end{vmatrix}. \tag{2}$$

The general solution for radial vibration and expressions for elements K_{ij} of the characteristic determinant are detailed in supplementary information (is available online at stacks.iop.org/SMS/30/055015/mmedia). Since the material properties (E, ν and ρ) are known for the three layers, the characteristic determinant Δ_R can be expressed as a function of natural frequency (radial mode) ω_r, and thickness of the corroded zinc oxide layer h_1 and the uncorroded zinc layer h_2, i.e. $\Delta_R = \Delta_R(\omega_r, h_1, h_2)$. Thus, the fundamental frequencies of a corroded system undergoing radial mode of vibration can be obtained by equating the characteristic determinant to zero. With thicknesses h_1 and h_2 obtained from Faraday's law of electrolysis, the characteristic equation $[\Delta_R(\omega_r) = 0]$ can be solved to obtain the natural frequency of a system undergoing radial vibration (mode shape of fundamental mode shown in figure 1(b)).

2.2. Mathematical formulation for transverse vibration of circular plates

As in case of section 2.1, the structure is modeled as a composite of two circular portions as shown in figure 2. The general solutions for displacement, shear angles as well as the equivalent geometrical and material rigidity properties for the individual portions are detailed in Supplementary Information.

For the two layer (zinc and zinc oxide) circular plate with equivalent circular PZT patch undergoing transverse vibration, the free edge boundary conditions at $r = a$ are:

- $M_{r1} = 0$ (moment free) i.e.

$$\frac{\partial \Phi_{r1}}{\partial r}\Big|_{r=a} + \frac{\nu_{1Teq}}{r}\left(\phi_{r1} + \frac{\partial \phi_{\theta 1}}{\partial \theta}\right)\Big|_{r=a} = 0, \tag{3}$$

- $M_{r\theta 1} = 0$ (moment free) i.e.

$$\frac{\partial \Phi_{\theta 1}}{\partial r}\Big|_{r=a} + \frac{1}{r}\left(\frac{\partial \phi_{r1}}{\partial \theta} - \phi_{\theta 1}\right)\Big|_{r=a} = 0 \tag{4}$$

- $Q_{r1} = 0$ (zero shear force) i.e.

$$\frac{\partial W_1}{\partial r}\Big|_{r=a} + \phi_{r1}\Big|_{r=a} = 0. \tag{5}$$

At the interface between Portion I and Portion II at $r = b$, there exists continuity of transverse displacement, shear angles, moments and shear forces i.e.

- Equal displacement

$$W_1\Big|_{r=b} = W_2\Big|_{r=b} \tag{6}$$

- Equal shear angles

$$\phi_{r1}\Big|_{r=b} = \phi_{r2}\Big|_{r=b} \tag{7}$$

$$\phi_{\theta 1}\Big|_{r=b} = \phi_{\theta 2}\Big|_{r=b} \tag{8}$$

- Equal moments

$$M_{r1}\Big|_{r=b} = M_{r2}\Big|_{r=b} \tag{9}$$

$$M_{r\theta 1}\Big|_{r=b} = M_{r\theta 2}\Big|_{r=b} \tag{10}$$

- Equal shear force

$$Q_{r1}\Big|_{r=b} = Q_{r2}\Big|_{r=b}. \tag{11}$$

Substituting the expressions for displacements and shear angles in equations (3)–(11) above, a 9×9 characteristic determinant is obtained as below:

$$\Delta_T = \begin{pmatrix} Q_{11} & Q_{12} & \cdots & Q_{19} \\ Q_{21} & Q_{22} & \cdots & Q_{29} \\ \vdots & \vdots & \ddots & \vdots \\ Q_{91} & Q_{92} & \cdots & Q_{99} \end{pmatrix} \tag{12}$$

where the non-zero elements Q_{ij} of the characteristic determinant are detailed in supplementary information. Since the material properties (E, ν and ρ) are known for the three layers, the characteristic determinant Δ_T can be expressed as a function of the natural resonance frequency of transverse vibration ω_t, and thickness of the corroded (zinc oxide) layer h_1 and the uncorroded (zinc) layer h_2, i.e. $\Delta_T = \Delta_T(\omega_t, h_1, h_2)$. Thus, the fundamental frequencies of a corroded system undergoing transverse vibration can be obtained by equating the characteristic determinant to zero. The thicknesses h_1 and h_2 are obtained from Faraday's law of electrolysis. With values of h_1 and h_2 thus determined, the characteristic equation can be expressed as $\Delta_T(\omega_t) = 0$. This transcendental equation is solved numerically to obtain the value of the natural resonance frequency (mode shape of fundamental mode shown in figure 1(c)).

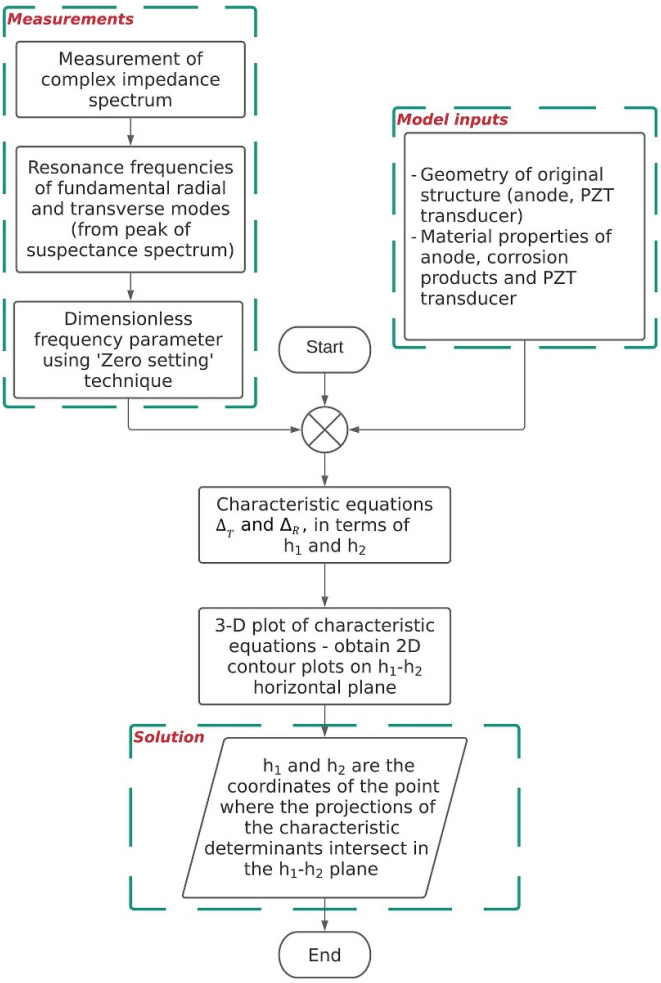

Figure 3. Flowchart of graphical inverse technique algorithm.

3. Graphical technique

3.1. Inverse problem

For a given circular anode with known PZT transducer size, the material properties (E, ν and ρ) are known for all three layers. Thus, the characteristic determinants Δ_R and Δ_T can be expressed as functions of the natural frequencies ω_r and ω_t, thickness of (uncorroded) metal anode layer h_2 and the thickness of (corroded) metal oxide layer h_1, i.e. $\Delta_R = \Delta_R(\omega_r, h_1, h_2)$ and $\Delta_T = \Delta_T(\omega_t, h_1, h_2)$. The natural frequencies (radial mode ω_r and transverse mode ω_t) are easily measured experimentally, allowing us to express the characteristic determinants as functions of h_1 and h_2: $\Delta_R = \Delta_R(h_1, h_2)$ and $\Delta_T = \Delta_T(h_1, h_2)$, i.e. a set of two non-linear equations in two variables. The system can be visualized in a 3D plot, by plotting the characteristic determinant (Δ_R or Δ_T) in the vertical direction (z-axis) with h_1 and h_2 in the two orthogonal directions in the horizontal plane for a measured natural frequency. Thus for a particular mode, a three-dimensional surface will be generated. Intersection of the horizontal plane at $\Delta = 0$ with the generated surface (projection on the $x-y$ i.e. $h_1 - h_2$ plane) yields all combinations of h_1 and h_2 that correspond to solutions of the characteristic determinant for the measured natural frequency. Given that we have two unknown parameters whose values need to be determined (h_1 and h_2), we require a minimum of two curves i.e. measurement of natural resonance frequencies of at least two modes is necessary. The coordinates of the intersection point of these 2D projections in the $x-y$ plane correspond to the solutions for h_1 and h_2.

Table 1. Non-zero elements in elastic stiffness matrix C_{ij} matrix of PZT-5H.

Elastic stiffness coefficient	Value (GPa)
$C_{11} = C_{22}$	127.205
C_{33}	117.436
$C_{12} = C_{21}$	80.212
$C_{13} = C_{31} = C_{23} = C_{32}$	84.670
$C_{44} = C_{55}$	22.989
C_{66}	23.474

Table 2. Material properties of Zn, ZnO and PZT-5H used for graphical inverse technique.

Material	Density (g cm^{-3})	Young's modulus (GPa)	Poisson's ratio
Zn	7.14	101.5	0.253
ZnO	5.68	210	0.33
PZT-5 H	7.5	60.6	0.289

3.2. Zero setting technique

The radius of the circular disc a is a critical input that determines the values of solutions to the characteristic equations of each mode for the plate undergoing corrosion. The value of the radius used for the calculation is determined using the 'zero setting' technique described here. This involves two sets of frequency parameters: the theoretical dimensionless frequency parameter for the uncorroded plate λ_{uct}, and the measured dimensionless frequency parameter λ_{ucm}. While λ_{uct} for an uncorroded circular disc is known, λ_{ucm} is determined from the measured uncorroded natural frequency (e.g. transverse mode ω_{tucm}) using the formula:

$$\lambda_{\text{ucm}}^4 = \frac{\rho h a^4}{D_T}\omega_{\text{tucm}}^2 \tag{13}$$

where all parameters and dimensions correspond to the metal anode before initiation of corrosion. The value of λ_{ucm} may differ from λ_{uct} due to simplifications arising from assumptions made in the analytical models for vibration analysis of circular plates. This necessitates 'zero setting' wherein the radius of the circular disc a is adjusted so that:

$$\lambda_{\text{uct}}^4 = \frac{\rho h a_{\text{adj}}^4}{D_T}\omega_{\text{tucm}}^2. \tag{14}$$

The value of a_{adj} thus determined is used as input to the characteristic equation. The same is extended to radial mode of vibration:

Table 3. Convergence study: impact of mesh settings in COMSOL multiphysics on convergence of solutions.

Mesh setting	Number of domain elements	Computation time (s)	Radial mode (kHz)	Transverse mode (kHz)
Extremely coarse	442	8	69.47	30.96
Extra coarse	2 029	8	69.43	30.60
Coarser	4 599	14	69.43	30.54
Coarse	10 067	28	69.42	30.51
Normal	18 853	54	69.42	30.49
Fine	29 472	86	69.42	30.49
Finer	48 407	165	69.42	30.49
Extra fine	109 222	444	69.42	30.49

Table 4. Comparison of FEA and analytical models.

Mode	FEM result, square shaped PZT (kHz)	Analytical result, equivalent isotropic circular PZT (kHz)	% Error
Radial	69.42	69.38	0.05
Transverse	30.49	30.31	0.59

Table 5. Comparison of estimated dimensionless thickness ratios using obtained frequencies from FE simulations with programmed dimensionless thickness ratios.

Case	Programmed μ_{uncorr}	Programmed μ_{corr}	Estimated μ_{uncorr}	Estimated μ_{corr}
1	0.99	0.016	0.994	0.015
2	0.99	0.009	0.992	0.009
3	0.99	0.003	0.991	0.003
4	0.95	0.078	0.963	0.074
5	0.95	0.047	0.959	0.045
6	0.95	0.016	0.954	0.015
7	0.90	0.157	0.919	0.146
8	0.90	0.094	0.914	0.089
9	0.90	0.031	0.906	0.030
10	0.80	0.313	0.829	0.286
11	0.80	0.188	0.819	0.174
12	0.80	0.062	0.809	0.059
13	0.70	0.469	0.740	0.433
14	0.70	0.282	0.726	0.258
15	0.70	0.094	0.712	0.087
16	0.60	0.626	0.648	0.592
17	0.60	0.376	0.633	0.345
18	0.60	0.125	0.615	0.114
19	0.50	0.783	0.547	0.763
20	0.50	0.469	0.538	0.439

$$\beta_{\text{uct}}^2 = \frac{\rho(1-\nu^2)a_{\text{adj}}^2}{E}\omega_{\text{rucm}}^2. \tag{15}$$

The value of a_{adj} are computed individually for both the transverse and radial mode of vibration. Figure 3 provides a schematic overview of the graphical technique, listing out individual steps involved in determination of solutions h_1 and h_2. In marine applications, the sacrificial anode is kept in vicinity of the structure under water and thus experiences free edge boundary condition. The natural frequencies of structures in contact with or immersed in water, decrease significantly in comparison with the natural frequencies in air [30]. The surrounding water introduces an additional virtual mass to the system which in turn reduces the natural frequency of the anode. However, the added virtual mass incremental (AVMI) factor, which is a function of the mode of vibration and the boundary condition, is reported to be least dominant for free edge circular plates [30]. Moreover, the *Zero Setting* technique accounts for the AVMI factor by means of a_{adj} and thus ensures accuracy of the graphical inverse technique.

4. Validation of graphical technique

For easier visualization of the results for various degree of corrosion, we introduce the following dimensionless quantities to represent thicknesses h_1 and h_2 normalized to h, the initial thickness of the metal anode before initiation of corrosion:

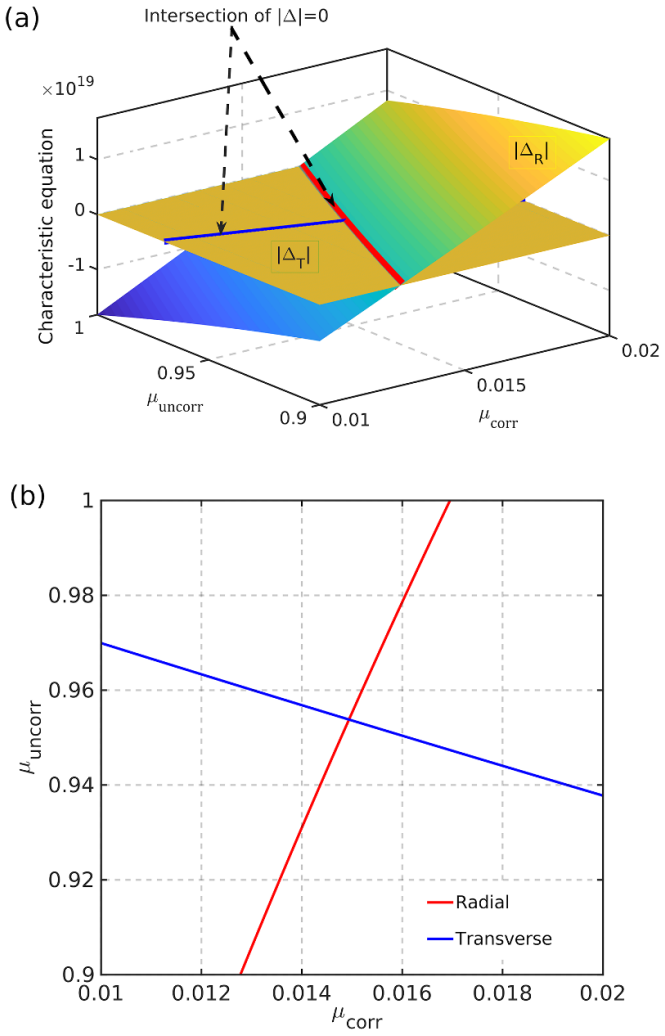

Figure 4. Representative plots corresponding to case no. 6 in table 5: (a) 3D plots of Δ_R and Δ_T, (b) equivalent 2D projections in $\mu_{\text{corr}} - \mu_{\text{uncorr}}$ plane, wherein the intersection point provides the estimated thickness ratios.

- Uncorroded thickness ratio:

$$\mu_{\text{uncorr}} = \frac{h_2}{h} \tag{16}$$

- Corroded thickness ratio:

$$\mu_{\text{corr}} = \frac{h_1}{h}. \tag{17}$$

4.1. Finite element analysis (FEA)

To validate the accuracy of the graphical inverse technique for determination of h_1 and h_2 from resonance frequency measurements, we apply the technique to results obtained from FEA performed using COMSOL Multiphysics.

As detailed in section 3, the material properties (E, ν, ρ) are inputs for the graphical inverse technique. The PZT-5H material is anisotropic in nature and elements of the elasticity matrix are provided in table 1. Solving the constitutive relations for a

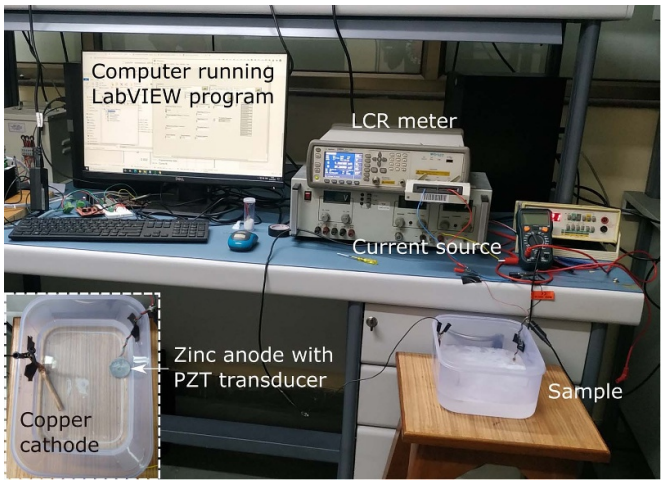

Figure 5. Experimental setup for accelerated corrosion of sacrificial zinc anode. Inset shows the sacrificial zinc anode sample instrumented with PZT transducer and a copper tube that serves as the cathode. 3.5% NaCl solution is used as the electrolyte in the electrolytic half-cell.

3D anisotropic material, we obtain the values of Young's modulus and Poisson's ratio in the three directions as:

$$E_1 = E_2 = 60.606 \text{ GPa} \tag{18}$$

$$E_3 = 48.309 \text{ GPa} \tag{19}$$

$$\nu_{12} = 0.289 \tag{20}$$

$$\nu_{13} = \nu_{23} = 0.512. \tag{21}$$

The thickness/length ratio of the PZT transducer is 0.02 and the ratio of thickness of PZT-5H to that of the zinc sacrificial anode is 0.055. Since the PZT is relatively very thin as compared to the zinc anode, the model is simplified by modeling the PZT transducer as an isotropic plate considering the Young's modulus and Poisson's ratio in $X - Y$ plane and neglecting the variation in Z-direction. The material properties of Zn, ZnO and equivalent isotropic PZT-5H material are listed in table 2.

Table 3 provides a comparison of the computation time and number of domain elements for various mesh settings available in COMSOL Multiphysics. The solutions for the radial and transverse mode eigenfrequencies for the zinc sacrificial anode converge for mesh settings beyond *Coarser*. The FE simulations are therefore performed using *Normal* mesh setting. The computation time is obtained on a computer with 64-bit Intel® Core(TM)-i7-7700HQ 2.80 GHz CPU and 16 GB RAM. However, the computation time increases significantly upon introduction of the zinc oxide layer. Table 4 compares resonance frequencies of fundamental radial mode and transverse mode obtained from FE simulations performed on the anode with square shaped anisotropic PZT model (figure 2(a))

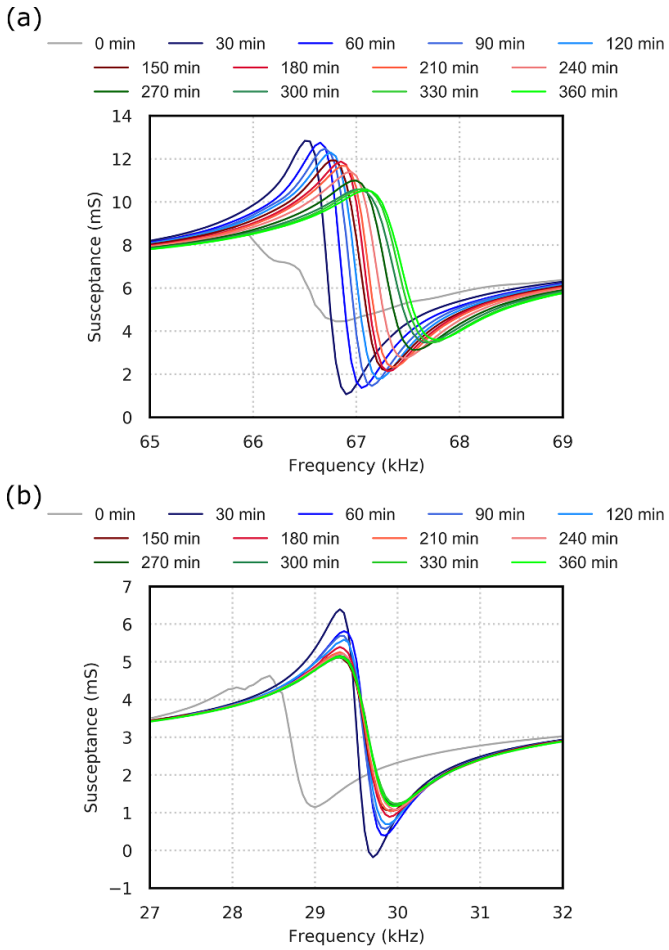

Figure 6. Susceptance spectra for (a) fundamental radial mode, and (b) fundamental transverse mode of one of the samples (sample A) undergoing accelerated corrosion. Impressed current of magnitude 0.35 A is applied to induce accelerated corrosion of the zinc anode, and the susceptance spectra for both modes are recorded at intervals of 30 min for duration of 6 h.

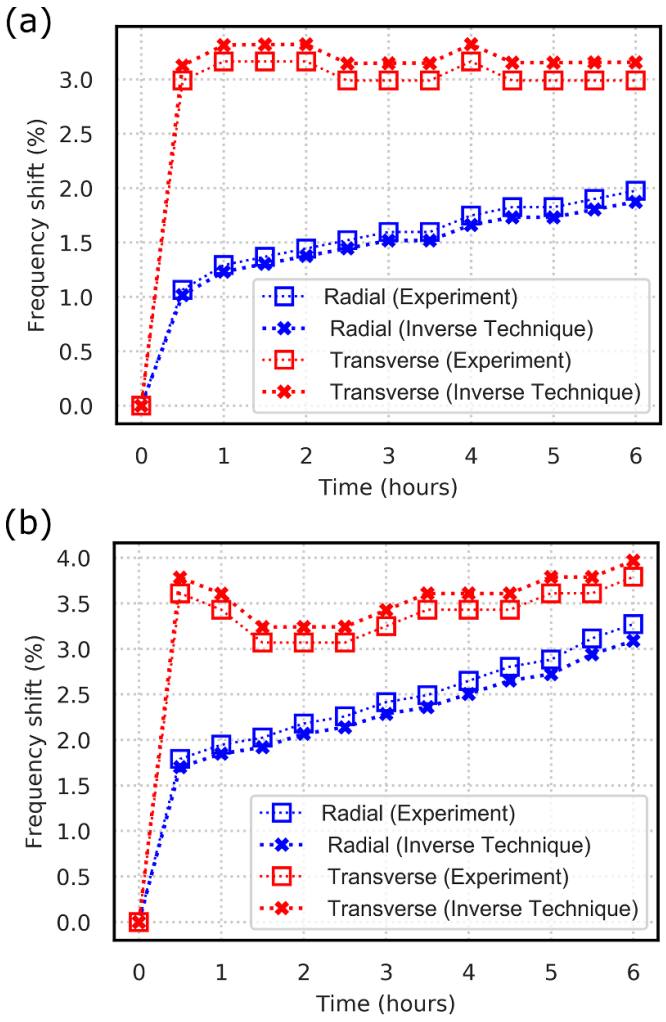

Figure 7. Frequency shift for fundamental radial mode and fundamental transverse vibration mode for (a) sample A, and (b) sample B. The series resonance frequencies (corresponding to peak susceptance in figure 6) measured every 30 min are programmed as inputs to the inverse graphical technique algorithm, to numerically estimate the thicknesses of Zn layer (h_2) and ZnO layer (h_1). To validate the accuracy of these estimated thickness values, we program them into an FE model in COMSOL Multiphysics and see excellent agreement of shift in eigenfrequency obtained from FEA (labeled 'Inverse Technique') to experimental results (labeled 'Experiment').

and solution of the analytical model assuming equivalent isotropic circular PZT transducer (figure 2(b)).

Table 5 lists the combinations of h_1 (μ_{corr}) and h_2 (μ_{uncorr}) programmed into COMSOL Multiphysics. We solve for the eigenfrequency values of the fundamental radial and fundamental transverse modes, whose mode shapes are shown in figures 1(b) and (c) respectively. These eigenfrequency values are then used to graphically find the solutions of the projection of the characteristic determinant in the $x-y$ i.e. $\mu_{\text{corr}}-\mu_{\text{uncorr}}$ plane. The estimated values of μ_{corr} and μ_{uncorr} thus obtained show excellent agreement with the programmed values as shown in table 5, with errors consistently less than 5%. A representative example of intersection of the two 3D surfaces and equivalent 2D contour plots are shown in figure 4, corresponding to case no. 6 in table 5.

4.2. Experimental results: corrosion monitoring of sacrificial zinc anodes

Two samples (A and B) of sacrificial anode with PZT transducer as described in section 2 are fabricated. The circular surface of the zinc anode is polished with fine grit sandpaper and square PZT transducer is attached using Fewikwik® instant adhesive at the center of the polished surface. Water-proofing of the surface housing the PZT transducer is achieved by applying epoxy sealant (M-Seal® Clear RTV Silicone Sealant) that is allowed to cure for 12 h. The assembly is subjected to accelerated corrosion induced by impressed current. The experimental setup consists of an electrolytic cell with a set of two electrodes (namely, a copper tube that serves as cathode, and the sacrificial zinc anode sample that serves as anode) submerged in an electrolyte (3.5% NaCl solution). The copper electrode is connected to negative terminal of a constant current source (Aplab LQ6324T, set to 0.35 A) while positive terminal of the current source is connected

Table 6. Thickness of Zn (h_2) and ZnO (h_1) layers estimated from resonance frequencies of sample A.

Time (min)	Fundamental radial mode (kHz)	Fundamental transverse mode (kHz)	Estimated h_2 (mm)	Estimated h_1 (mm)
0	65.80	28.45	7.300	0.000
30	66.50	29.30	7.248	0.111
60	66.65	29.35	7.196	0.133
90	66.70	29.35	7.173	0.140
120	66.75	29.35	7.151	0.147
150	66.80	29.30	7.112	0.154
180	66.85	29.30	7.090	0.161
210	66.85	29.30	7.090	0.161
240	66.95	29.35	7.061	0.175
270	67.00	29.30	7.025	0.181
300	67.00	29.30	7.025	0.181
330	67.05	29.30	7.003	0.188
360	67.10	29.30	6.982	0.195

Table 7. Thickness of Zn (h_2) and ZnO (h_1) layers estimated from resonance frequencies of sample B.

Time (min)	Fundamental radial mode (kHz)	Fundamental transverse mode (kHz)	Estimated h_2 (mm)	Estimated h_1 (mm)
0	64.20	27.70	7.300	0.000
30	65.35	28.70	7.092	0.182
60	65.45	28.65	7.031	0.195
90	65.50	28.55	6.976	0.200
120	65.60	28.55	6.934	0.214
150	65.65	28.55	6.913	0.221
180	65.75	28.60	6.887	0.236
210	65.80	28.65	6.883	0.245
240	65.90	28.65	6.842	0.258
270	66.00	28.65	6.802	0.272
300	66.05	28.70	6.798	0.280
330	66.20	28.70	6.740	0.301
360	66.30	28.75	6.717	0.316

to the zinc anode. The impedance of the PZT transducer is measured using a precision LCR meter (Agilent E4980A). The LCR meter is connected to a computer, and is controlled using a custom-made software designed with LabVIEW for data acquisition. A photograph of the experimental setup is shown in figure 5. At every 30 min interval, the current source is turned off and impedance of the PZT transducer is recorded, without disturbing the mechanical arrangement of the apparatus. The electromechanical resonance frequency is obtained from the susceptance spectra recorded using a LabVIEW program running on a computer connected to the LCR meter. Figure 6 shows experimentally measured change in susceptance spectra for the fundamental radial and fundamental transverse modes of vibration over duration of the experiment. The series resonance frequencies for the fundamental radial and fundamental transverse mode (corresponding to peak susceptance in figure 6) measured every 30 min are programmed as inputs to the inverse technique algorithm, to numerically estimate (using MATLAB) the thicknesses of Zn layer (h_2) and ZnO layer (h_1). To validate the accuracy of these estimated thickness values, we program them into an FE model in COMSOL Multiphysics and see excellent agreement of shift in eigenfrequency obtained from COMSOL Multiphysics to experimental result for each mode, as shown in figure 7. Tables 6 and 7 show estimated thickness of Zn and ZnO layer for every time interval from the inverse technique for sample A and sample B respectively.

5. Discussion and conclusion

In summary, this paper presents a formulation for natural vibration analysis of a sacrificial anode (shaped in form of a thick circular plate) with PZT transducer undergoing corrosion. The graphical technique for inverse problems for crack and delamination size quantification in beams has been extended to the detection and quantification of extend of corrosion in circular thick plates. The analysis is based on the 'constrained model', where both corroded and uncorroded layers are assumed to be rigidly coupled with each other i.e.

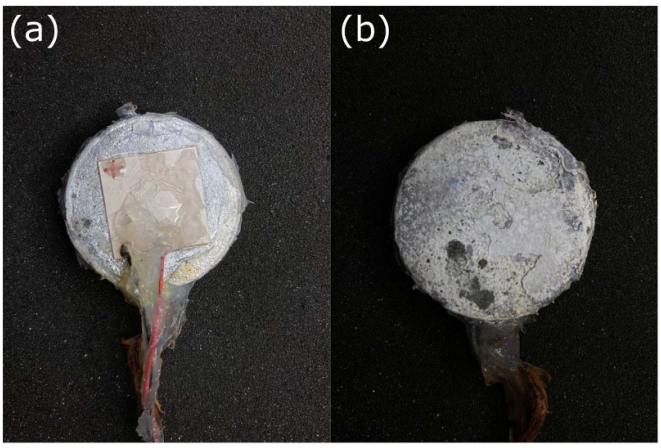

Figure 8. Photograph of a corroded canode showing the (a) top surface protected by epoxy sealant, and (b) non-uniform corrosion of the bottom surface. The epoxy sealant is peeled off for better visualization of the uncorroded top surface following application of impressed current for 360 min.

both layer have equal transverse and radial displacement. As described in section 4, the graphical technique provides an excellent estimation of thickness of corroded and uncorroded layers of the sacrificial anode, thereby making it possible to estimate extent of corrosion i.e. health of the anode. The model presented in section 2 assumes uniform corrosion of the bottom surface of the anode (i.e. opposite surface as the one on which the PZT transducer is attached). Even though the accelerated corrosion induced by impressed current results in non-uniform corrosion of the anode (as shown in figure 8), the graphical technique with uniform-corrosion model shows excellent agreement with the trend seen in experimental results as shown in figure 7. The varying extents of corrosion induced in samples A and B (as detailed in tables 6 and 7) are attributed to manual setup of the components involved in the experiment, that could result in variation in current efficiency during electrolysis and partial delamination of the zinc oxide layer [27]. The graphical technique could be further improved by incorporating the anisotropic nature of the piezoelectric material. The AVMI factor decreases for higher modes of vibration and thus reduces the effect of water loading on the resonance frequencies [30] . However, the experimental setup was limited to frequencies up to 100 kHz and hence higher frequency modes could not be leveraged in this experiment. As compared to our earlier work [27], the graphical technique does not require in-field calibration i.e. empirical model of delamination dynamics of the ZnO layer and quantification of the corrosion current efficiency (Faradaic efficiency). Therefore, the technique proposed in this paper can be used for in-situ monitoring of sacrificial anodes and quantifying cover deterioration due to corrosive agents in marine infrastructure prone to corrosion. This technique is cost-effective and can be equipped with portable impedance analyzers (e.g. Analog Devices AD5933) and remote monitoring capabilities and thus has wide application potential in SHM. The technique presented in this work will also be useful in obtaining thickness of films in MEMS resonator based gravimetric sensing.

Acknowledgments

This work was supported by IMPRINT-2A by Department of Science & Technology, Government of India [Grant IMP/2018/001442] with additional financial support from Sanrachana Structural Strengthening Pvt. Ltd [Grant RD/0119-SSIMPQ2-001]. The authors thank Krishna Conchem Products Pvt. Ltd for providing the zinc sacrificial anodes used for performing the experiments, Mr Hrishikesh Belatikar at IIT Bombay for assistance with developing LabVIEW based data acquisition software, and Wadhwani Electronics Lab (WEL) at IIT Bombay for providing Agilent E4980A precision LCR meter.

ORCID iDs

Jeslin Thalapil https://orcid.org/0000-0003-2236-2750
Siddharth Tallur https://orcid.org/0000-0003-1399-2187

References

[1] Ballantine Jr D, White R M, Martin S J, Ricco A J, Zellers E, Frye G, and Wohltjen H 1996 *Acoustic Wave Sensors: Theory, Design and Physico-Chemical Applications* (Amsterdam: Elsevier)
[2] Benetti M, Cannata D, Di Pietrantonio F, Foglietti V and Verona E 2005 Microbalance chemical sensor based on thin-film bulk acoustic wave resonators *Appl. Phys. Lett.* **87** 173504
[3] Zhang H and Kim E S 2005 Micromachined acoustic resonant mass sensor *J. Microelectromech. Syst.* **14** 699
[4] Rey-Mermet S, Lanz R and Muralt P 2006 Bulk acoustic wave resonator operating at 8 GHz for gravimetric sensing of organic films *Sensors Actuators* B **114** 681
[5] Rabus D, Friedt J, Ballandras S, Baron T, Lebrasseur E and Carry E 2015 High-overtone bulk-acoustic resonator gravimetric sensitivity: towards wideband acoustic spectroscopy *J. Appl. Phys.* **118** 114505
[6] Talakokula V, Bhalla S, Ball R, Bowen C, Pesce G, Kurchania R, Bhattacharjee B, Gupta A and Paine K 2016 Diagnosis of carbonation induced corrosion initiation and progression in reinforced concrete structures using piezo-impedance transducers *Sensors Actuators* A **242** 79
[7] Talakokula V, Bhalla S and Gupta A 2018 Monitoring early hydration of reinforced concrete structures using structural parameters identified by piezo sensors via electromechanical impedance technique *Mech. Syst. Signal Process.* **99** 129
[8] Li W, Liu T, Zou D, Wang J and Yi T-H 2019 PZT based smart corrosion coupon using electromechanical impedance *Mech. Syst. Signal Process.* **129** 455
[9] Yoon H, Youn B D and Kim H S 2016 Kirchhoff plate theory-based electromechanically-coupled analytical model considering inertia and stiffness effects of a surface-bonded piezoelectric patch *Smart Mater. Struct.* **25** 025017
[10] Li W, Wang J, Liu T and Luo M 2020 Electromechanical impedance instrumented circular piezoelectric-metal transducer for corrosion monitoring: modeling and validation *Smart Mater. Struct.* **29** 035008
[11] Wang Q, Quek S, Sun C and Liu X 2001 Analysis of piezoelectric coupled circular plate *Smart Mater. Struct.* **10** 229
[12] Liu Y and Feng X 2020 Monitoring corrosion-induced thickness loss of stainless steel plates using the

electromechanical impedance technique *Meas. Sci. Technol.* **32** 025104
[13] Salawu O 1997 Detection of structural damage through changes in frequency: a review *Eng. Struct.* **19** 718
[14] Ravi J, Nidhan S, Muthu N and Maiti S 2018 Analytical and experimental studies on detection of longitudinal, L and inverted T cracks in isotropic and bi-material beams based on changes in natural frequencies *Mech. Syst. Signal Process.* **101** 67
[15] Chondros T and Dimarogonas A 1980 Identification of cracks in welded joints of complex structures *J. Sound Vib.* **69** 531
[16] Gasch R 1993 A survey of the dynamic behaviour of a simple rotating shaft with a transverse crack *J. Sound Vib.* **160** 313
[17] Doebling S, Farrar C and Prime M 1998 A summary review of vibration-based damage identification methods *Shock Vib. Dig.* **30** 91
[18] Bachschmid N, Pennacchi P and Tanzi E 2010 *Cracked Rotors* (Berlin: Springer)
[19] Wu X, Ghaboussi J and Garrett J 1992 Use of neural networks in detection of structural damage *Comput. Struct.* **42** 649
[20] Valoor M T and Chandrashekhara K 2000 A thick composite-beam model for delamination prediction by the use of neural networks *Compos. Sci. Technol.* **60** 1773
[21] Chou J-H and Ghaboussi J 2001 Genetic algorithm in structural damage detection *Comput. Struct.* **79** 1335
[22] Rao M, Srinivas J and Murthy B 2004 Damage detection in vibrating bodies using genetic algorithms *Comput. Struct.* **82** 963
[23] Adams R D, Cawley P, Pye C J and Stone B J 1978 A vibration technique for non-destructively assessing the integrity of structures *J. Mech. Eng. Sci.* **20** 93
[24] Zhang Z, Shankar K, Ray T, Morozov E V and Tahtali M 2013 Vibration-based inverse algorithms for detection of delamination in composites *Compos. Struct.* **102** 226
[25] Nandwana B and Maiti S 1997 Modelling of vibration of beam in presence of inclined edge or internal crack for its possible detection based on frequency measurements *Eng. Fract. Mech.* **58** 193
[26] Thalapil J and Maiti S 2014 Detection of longitudinal cracks in long and short beams using changes in natural frequencies *Int. J. Mech. Sci.* **83** 38
[27] Tamhane D, Thalapil J, Banerjee S and Tallur S 2021 Smart cathodic protection system for real-time quantitative assessment of corrosion of sacrificial anode based on electro-mechanical impedance (EMI) *IEEE Access* **9** 12230
[28] Mujumdar P and Suryanarayan S 1988 Flexural vibrations of beams with delaminations *J. Sound Vib.* **125** 441
[29] Meng Y, Liu L, Zhang D, Dong C, Yan Y, Volinsky A A and Wang L-N 2019 Initial formation of corrosion products on pure zinc in saline solution *Bioact. Mater.* **4** 87
[30] Kwak M K 1991 Vibration of circular plates in contact with water *Trans. ASME* E **58** 480